The Astrophysical Journal, 982:19 (10pp), 2025 March 20 https://doi.org/10.3847/1538-4357/adb711

Signature of Strange Star as the Central Engine of GRB 240529A

Xiao Tian[1], HouJun Lü[1], WenJun Tan[2], ShaoLin Xiong[2], HaoYu Yuan[3], WenYuan Yu[1], ShuQing Zhong[4], WenLong Zhang[2,5], and EnWei Liang[1]
[1] Guangxi Key Laboratory for Relativistic Astrophysics, Department of Physics, Guangxi University, Nanning 530004, People's Republic of China; lhj@gxu.edu.cn
[2] Key Laboratory of Particle Astrophysics, Institute of High Energy Physics, Chinese Academy of Sciences, Beijing 100049, People's Republic of China
[3] Department of Astronomy, School of Physics, Huazhong University of Science and Technology, Wuhan, 430074, People's Republic of China
[4] School of Science, Guangxi University of Science and Technology, Liuzhou 545006, People's Republic of China
[5] School of Physics and Physical Engineering, Qufu Normal University, Qufu 273165, People's Republic of China
Received 2024 August 6; revised 2025 February 10; accepted 2025 February 16; published 2025 March 12

Abstract

GRB 240529A is a long-duration gamma-ray burst (GRB) whose light curve of prompt emission is composed of a triple-episode structure, separated by quiescent gaps of tens to hundreds of seconds. More interestingly, its X-ray light curve of afterglow exhibits two plateau emissions, namely, an internal plateau emission that is smoothly connected with a $\sim t^{-0.1}$ segment and followed by a $\sim t^{-2}$ power-law decay. The three episodes in the prompt emission, together with two plateau emissions in X-ray, are unique in the Swift era. They are very difficult to explain with the standard internal/external shock model by invoking a black hole central engine. However, it could be consistent with the prediction of a supramassive magnetar as the central engine, the physical process of phase transition from a magnetar to a strange star, as well as the cooling and spin-down of the strange star. In this paper, we propose that the first- and second-episode emissions in the prompt gamma ray of GRB 240529A are from the jet emission of a massive star collapsing into a supramassive magnetar and the reactivity of the central engine, respectively. Then, the third-episode emission of the prompt is attributed to the phase transition from a magnetar to a strange star. Finally, the first and second plateau emissions of the X-ray afterglow are powered by the cooling and spin-down of the strange star, respectively. The observational data of each component of GRB 240529A are roughly coincident with the estimations of the above physical picture.

Unified Astronomy Thesaurus concepts: Gamma-ray bursts (629)

1. Introduction

The central engine and energy extraction mechanism in gamma-ray bursts (GRBs) study remains an open question (B. Zhang 2011). The burst duration (T_{90}) of the prompt emission of GRBs ranges from 10 ms to several hours. Together with the measured redshift, one can roughly estimate the total isotropic energy, which ranges from (10^{48} to 10^{55}) erg (S. B. Cenko et al. 2011; P. Kumar & B. Zhang 2015). Based on the duration of the burst, GRBs can be roughly classified into long-duration GRBs (LGRBs, $T_{90} > 2$ s) and short-duration GRBs (SGRBs, $T_{90} < 2$ s) (C. Kouveliotou et al. 1993; O. Bromberg et al. 2013). Some LGRBs associated with core-collapse supernovae confirmed that at least some LGRBs originate from the collapse of massive stars (T. J. Galama et al. 1998; K. Z. Stanek et al. 2003; D. Malesani et al. 2004; M. Modjaz et al. 2006; E. Pian et al. 2006; B. Zhang 2006; P. L. Kelly et al. 2008; C. Raskin et al. 2008; H.-J. Lü et al. 2010; P. L. Kelly & R. P. Kirshner 2012; B. D. Metzger 2019), while the merger of binary compact stars may be the progenitor of SGRBs (B. Zhang 2006; H.-J. Lü et al. 2010; E. Berger et al. 2013; Z.-P. Jin et al. 2016; B. P. Abbott et al. 2017; H.-J. Lü et al. 2017; G. P. Lamb et al. 2019; B. D. Metzger 2019). Whether it is from a massive star collapse or the merger of binary compact stars, a hyperaccreting black hole (R. Popham et al. 1999; W.-H. Lei et al. 2013; T. Liu et al. 2017) or a rapidly spinning, strongly magnetized neutron star (millisecond magnetar) (V. V. Usov 1992; C. Thompson 1994; Z. G. Dai & T. Lu 1998a, 1998b; B. Zhang & P. Mészáros 2001; B. D. Metzger et al. 2011; N. Bucciantini et al. 2012; H.-J. Lü & B. Zhang 2014; H.-J. Lü et al. 2015) as the central engine of GRB, may survive after such catastrophic events to drive an extremely relativistic jet and produce GRB.

On the other hand, a strange star (SS) with an extremely high density has been proposed as the engine of GRBs by many authors (A. V. Olinto 1987; I. Bombaci et al. 2000; Z. Berezhiani et al. 2003; R. Ouyed et al. 2005; A. Li et al. 2016; A. Drago & G. Pagliara 2016; R. Ouyed et al. 2020). Even in the absence of compelling evidence for the existence of strange stars in the Universe, there is also no compelling reason why they should not exist. Moreover, the phase transition from neutron star (NS) to strange star (SS) (hereafter NS → SS phase transition) is also proposed as a potential energy source for GRBs (K. S. Cheng & Z. G. Dai 1996; Z. G. Dai & T. Lu 1998b; I. Bombaci et al. 2000; R. Ouyed & F. Sannino 2002; P. Haensel & J. L. Zdunik 2006). E. Witten (1984) pointed out that strange quark matter (SQM) is composed of nearly equal proportion of u, d, and s quarks, which are more stable than hadronic matter (F. Weber 2005; E. Farhi & R. L. Jaffe 1984). Different mechanisms of phase transition from NS → SS have been proposed (C. Alcock et al. 1986; A. V. Olinto 1987; K. S. Cheng & Z. G. Dai 1996; I. Bombaci et al. 2004; B. W. Mintz et al. 2010; M. Herzog & F. K. Röpke 2011; A. G. Pili et al. 2016; R. Ouyed et al. 2020), but all of them are based on a "seed" of SQM formed inside of a neutron star. The seeds of SQM can be produced via two mechanisms: one is from the early time after the Big Bang; the other is that the seeds are formed in the core of the neutron

star due to the NS → SS phase transition. The central density of a neutron star continuously increases via the accretion of material to increase gravity or loss of the rotation energy of a neutron star to decrease its centrifugal force. Once its central density reaches the critical density value of the quantum chromodynamics (QCD) phase transition, the NS will transition to an SS. This deconfinement phase transition lasts only a few milliseconds, but releases a total energy as high as $E_{\rm conv} = (1–4) \times 10^{53}$ erg, which is consistent with the observed gamma-ray energy of GRBs (I. Bombaci et al. 2000).

From the observational point of view, external plateaus with normal decay phases were later commonly observed in Swift early XRT light curves for both LGRBs and SGRBs (H.-J. Lü & B. Zhang 2014; H.-J. Lü et al. 2015). It can be interpreted as the energy injection into the external shock when a relativistic jet propagates into the circumburst medium (B. Zhang et al. 2006). However, a good fraction of Swift GRBs exhibit an X-ray plateau followed by a very sharp drop with a temporal decay slope steeper than 3, called an internal plateau (E. Troja et al. 2007; N. Lyons et al. 2010; A. Rowlinson et al. 2013; H.-J. Lü et al. 2017). Such rapid decay cannot be accommodated by any external shock model, but is consistent with a supramassive magnetar collapsing into a black hole (B. Zhang 2018) or energy injection from the latent heat released by the solidification of the newborn strange quark star into the GRB afterglow (S. Dai et al. 2011; S.-J. Hou et al. 2018).

Recently, a particular long-duration GRB 240529A was detected by Swift (R. A. J. Eyles-Ferris et al. 2024), Hard X-ray Modulation Telescope (Insight-HXMT; W. Tan et al. 2024), as well as the Konus-Wind (D. Svinkin et al. 2024). The prompt emission of GRB 240529A consists of a triple-episode structure with two long-duration gaps, which are quite similar to that of precursors observed in both Burst And Transient Source Experiment (T. M. Koshut et al. 1995) and Fermi/GBM (L. Lan et al. 2018; P. Coppin et al. 2020), while the X-ray afterglow light curve exhibits one steep decay and two plateau emissions. The characteristics of a two-plateau emission are difficult to explain by existing internal dissipation or external shock models. In this paper, we propose a supramassive magnetar as the central engine. Then, we invoke the physical process of magnetar collapse into a strange star, and the cooling and spin-down of the strange star to interpret both the prompt emission and X-ray afterglow of GRB 240529A. The systematic analysis of the observational data for GRB 240529A is shown in Section 2. In Section 3, we attempt to present a physical interpretation of each observed segment of GRB 240529A. The conclusions with some discussion are drawn in Section 4. Throughout the paper, we adopt the convention $Q = 10^{x}Q_{x}$ in cgs units, and employ a concordance cosmology with parameters $\Omega_M = 0.30$, $\Omega_\Lambda = 0.70$, and $H_0 = 70\,{\rm km\,s^{-1}\,Mpc^{-1}}$.

2. Data Reduction and Analysis

2.1. Swift/BAT Observations

At 02:58:31 UT on 2024 May 29 (as the T_0), the Swift Burst Alert Telescope (BAT) triggered and located GRB 240529A (R. A. J. Eyles-Ferris et al. 2024). We downloaded the BAT data from the Swift website[6] and used the standard HEASOFT tools (version 6.28) to process the BAT data. The BAT light curves in different energy bands are extracted with a fixed 1 s time bin. The light curve shows a single-episode structure with multiple pulses (see Figure 1), and the duration can be estimated as $T_{90,\rm BAT} = 161 \pm 15$ s in the 15–350 keV (C. B. Markwardt et al. 2024). The background is extracted using two time intervals before and after the burst, and then model the background as Poisson noise, which is the standard background model for prompt emission in BAT events. For more details, refer to T. Sakamoto et al. (2008). The time-averaged spectrum of the prompt emission observed by BAT is best fit by a simple power-law model with an index $\Gamma = 1.68 \pm 0.04$ (C. B. Markwardt et al. 2024) due to its narrow energy band.

2.2. Insight-HXMT Observations

Hard X-ray Modulation Telescope (Insight-HXMT) is the first X-ray astronomical satellite of China, and was successfully launched on 2017 June 15 (S.-N. Zhang et al. 2020). It has a very wide energy band from 1 keV to 3 MeV, and includes three kinds of main scientific payloads, such as High Energy X-ray telescope (HE), the Medium Energy X-ray telescope (ME), and the Low Energy X-ray telescope (LE; S.-N. Zhang et al. 2020).

At 02:51:44 UT on 2024 May 29 (corresponding to $T_0 - 407$ s), Insight-HXMT/HE detected GRB 240529A in a routine search of the data (W. Tan et al. 2024). It is earlier than the triggered time of Swift/BAT about 407 s. The Insight-HXMT/HE instrument is equipped with 18 cylindrical NaI (Tl)/CsI(Na) phoswich detectors with a total detection area of 5000 $\rm cm^2$. The NaI detectors are sensitive to hard X-rays in the 20–250 keV range, while the CsI detectors serve as anticoincidence detectors to mitigate upward background noise. Gamma-ray photons with energies exceeding 200 keV can penetrate the spacecraft and payload structure, leaving their signatures in the Insight-HXMT/HE system. Due to limitations in crystal thickness and the narrow field of view obstructed by collimators, detecting GRBs with NaI detectors is difficult. However, the CsI(Na) crystals, with their greater thickness, can record high-energy gamma-ray photons, thus one can detect the GRBs that are not occulted by the CsI detectors (Q. Luo et al. 2020).

Then, we extract the light curve of the prompt emission of GRB 240529A for all 18 CsI detectors in the 70–900 keV energy band with a time bin of 1 s. The light curve consists of a triple-episode structure with multiple pulses at $T_0 - 422$ s, $T_0 - 315$ s, and $T_0 - 67$ s, respectively (see Figure 1). The structure of the light curve is consistent with that of observations by Konus-Wind (D. Svinkin et al. 2024). The duration of those three episodes (marked as I, II, and III) with an energy range of (150–600) keV are $T_{90,\rm I} \sim 35$ s, $T_{90,\rm II} \sim 18$ s, and $T_{90,\rm III} \sim 180$ s, respectively.

Finally, we fit the data with a second-order polynomial to obtain a smooth background-subtracted light curve. For each episode (T_0-422 s to T_0-387 s, T_0-315 s to T_0-297 s, T_0-67 s to T_0+113 s), the spectra were extracted using all 18 detectors in the energy range of 150–600 keV, corresponding to the optimal effective area of the CsI detectors. The background was determined by interpolating the signal in two time intervals before and after the burst using a third-order polynomial. For more details, refer to Q. Luo et al. (2020). The time-averaged spectrum of the first two episodes is best fit by a simple power-

[6] https://www.swift.ac.uk/archive/selectseq.php?source=obs&tid=1231488

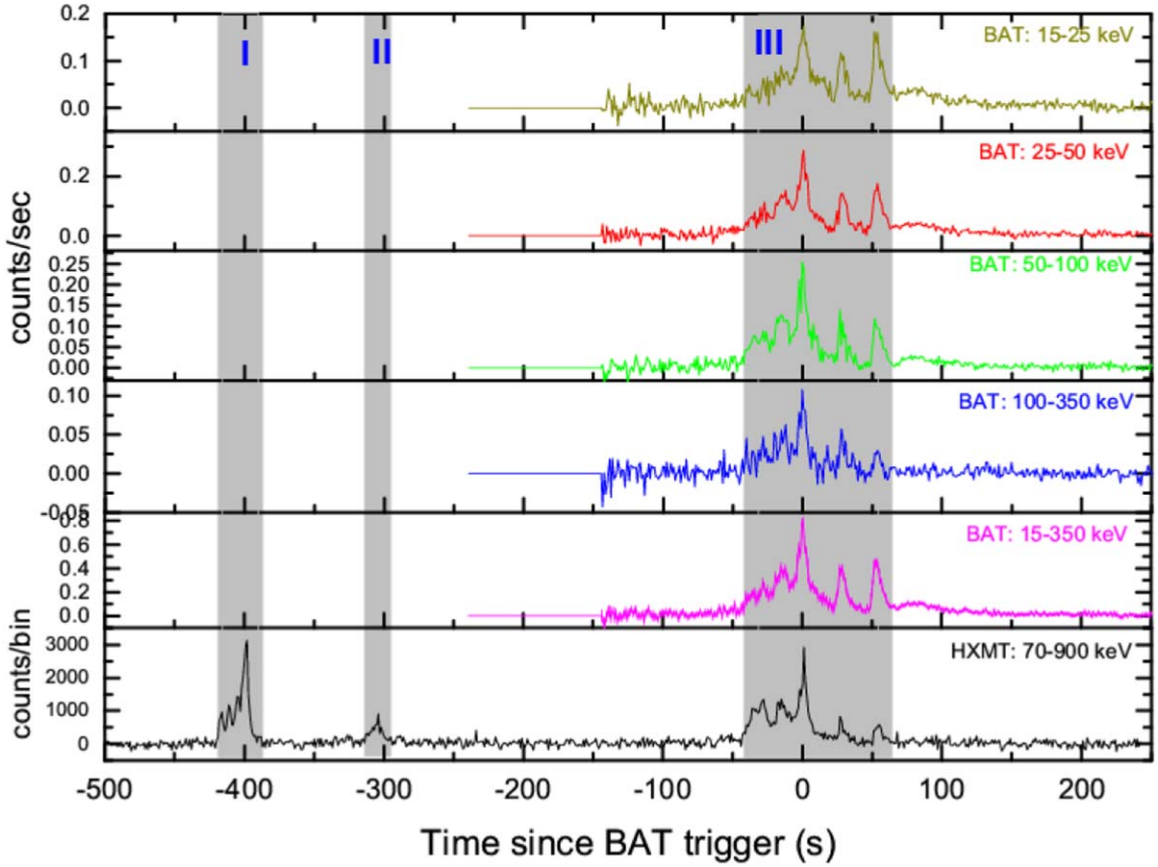

Figure 1. Swift/BAT and HXMT light curves of GRB 240529A in different energy bands with a 1.0 s time bin.

law model, which is expressed as

$$N_{\rm PL}(E) = A \cdot \left(\frac{E}{100\ {\rm keV}}\right)^{\Gamma}. \quad (1)$$

The power-law indices for the first two episodes are $\Gamma_{\rm I} = -1.59 \pm 0.03$ and $\Gamma_{\rm II} = -1.44 \pm 0.09$, respectively. The time-averaged spectrum of the third episode, together with Swift/BAT data, can be adequately fitted by a cutoff power-law model,

$$N_{\rm CPL}(E) = A \cdot \left(\frac{E}{100\ {\rm keV}}\right)^{\Gamma} \exp[-\frac{E(2+\Gamma)}{E_{\rm p}}], \quad (2)$$

and one can obtain the $\Gamma_{\rm III} = -1.38 \pm 0.04$ and $E_{\rm p} = 584^{+102}_{-74}$ keV. The fluence of those three episodes in 10–1000 keV are corresponding to $f_{\rm I} = (1.12 \pm 0.09) \times 10^{-5}\,{\rm erg\,cm^{-2}}$, $f_{\rm II} = (1.97 \pm 0.55) \times 10^{-6}\,{\rm erg\,cm^{-2}}$, and $f_{\rm III} = (3.00 \pm 0.04) \times 10^{-5}\,{\rm erg\,cm^{-2}}$, respectively.

2.3. Swift X-Ray Telescope Observations

We downloaded the X-ray telescope (XRT) data of GRB 240529A from the Swift archive,[7] and the XRT began observing the field at 107 s after the BAT trigger (S. Dichiara et al. 2024). Figure 2 shows the XRT light curve in the energy range from 0.3 to 10 keV. It is worth noting that the X-ray light curve of GRB 240529A seems to be interesting, and it is quite different from the canonical X-ray emission that is composed of four successive segments (J. A. Nousek et al. 2006; B. Zhang et al. 2006). It is composed of two plateau emission phases and one power-law segment. We perform an empirical fitting to the light curve with one steep decay of power law and two smooth broken power-law models, which can be expressed as (E.-W. Liang et al. 2007),

$$F_1 = F_{0,1}\left(\frac{t}{t_1}\right)^{-\alpha_1}, \quad (3)$$

$$F_2 = F_{0,2}\left[\left(\frac{t}{t_{\rm b,2}}\right)^{\omega_2\alpha_2} + \left(\frac{t}{t_{\rm b,2}}\right)^{\omega_2\alpha_3}\right]^{-1/\omega_2}, \quad (4)$$

$$F_3 = F_{0,3}\left[\left(\frac{t}{t_{\rm b,3}}\right)^{\omega_3\alpha_4} + \left(\frac{t}{t_{\rm b,3}}\right)^{\omega_3\alpha_5}\right]^{-1/\omega_3}. \quad (5)$$

The total X-ray light curve can be fitting by the superposition of those three models,

$$F = F_1 + F_2 + F_3. \quad (6)$$

Here, t_1 is the starting time of X-ray observations, $t_{\rm b,2}$ and $t_{\rm b,3}$ are the two break times for first and second plateau emissions. α_1 is the initial power-law decay index, α_2 and α_3 are the decay index before and after $t_{\rm b,2}$, and α_4 and α_5 are the decay index before and after $t_{\rm b,3}$. ω_2 and ω_3 describe the sharpness of the break at $t_{\rm b,2}$ and $t_{\rm b,3}$, and fixed with $\omega_2 = 10$ and $\omega_3 = 7$.

Then, we adopt a Markov Chain Monte Carlo (MCMC) method to fit the light curve by invoking the above one power law + two smooth broken power-law models. The fitting results of the X-ray light curve for GRB 240529A are shown in

[7] https://www.swift.ac.uk/xrt_curves/00998907/

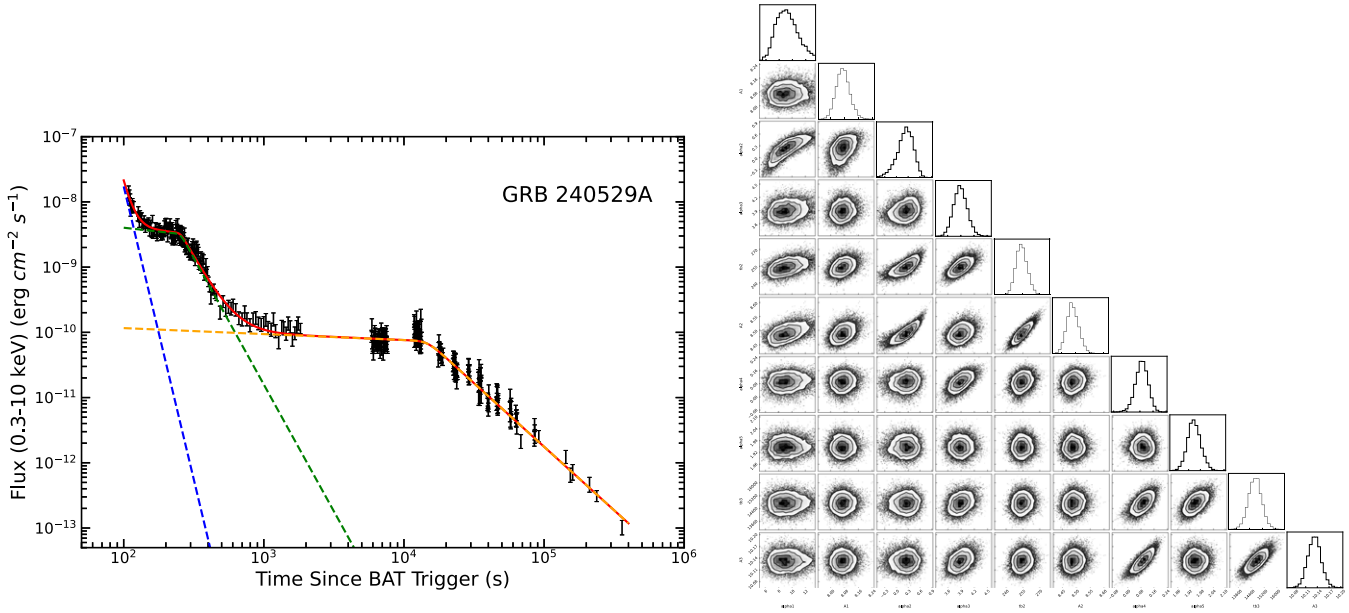

Figure 2. Left: XRT (black) light curve of GRB 240529A. The red solid line represents the total component fitting line. The blue, green, and orange dashed lines are the best-fitted lines for the power law and two plateaus, respectively. Right: corner plots and parameter constraints for the fitting parameters of the XRT light curve of GRB 240529A.

Table 1
Fitting Results of the X-Ray Afterglow Light Curves of GRB 240529A

	α	t_b (s)	F_b (erg cm^{-2} s^{-1})
Power law	$\alpha_1 = 9.09 \pm 1.45$		$(8.51 \pm 0.75) \times 10^{-9}$
First plateau	$\alpha_2 = 0.25 \pm 0.18$ $\alpha_3 = 3.89 \pm 0.15$	$t_{b,1} = 254 \pm 5$	$(3.02 \pm 0.14) \times 10^{-9}$
Second plateau	$\alpha_4 = 0.09 \pm 0.04$ $\alpha_5 = 1.95 \pm 0.03$	$t_{b,2} = 14703 \pm 401$	$(6.71 \pm 0.30) \times 10^{-11}$

Figure 2, as well as the corner plots of constrained parameters. The first segment is a power-law decay with the temporal index $\alpha_1 = 9.09 \pm 1.45$, which is consistent with the tail emission of a prompt gamma ray from the curvature effect (P. Kumar & A. Panaitescu 2000; B.-B. Zhang et al. 2007; Z. L. Uhm & B. Zhang 2015). Two plateaus primarily dominate the XRT light curve of GRB 240529A. The first plateau exhibits a shallow decay phase followed by a rapid decay phase with the temporal index $\alpha_2 = 0.25 \pm 0.18$ and $\alpha_3 = 3.89 \pm 0.15$, and the break time is $t_{b,2} = 254 \pm 5$ s. In the second plateau, the temporal decay index before and after the break time $t_{b,3} = 14703 \pm 401$ s are $\alpha_4 = 0.09 \pm 0.04$ and $\alpha_5 = 1.95 \pm 0.03$, respectively. The peak flux at the break time of the two plateaus is $F_{b,2} = (3.02 \pm 0.14) \times 10^{-9}$ erg cm^{-2} s^{-1} and $F_{b,3} = (6.71 \pm 0.30) \times 10^{-11}$ erg cm^{-2} s^{-1}, respectively. This fitting parameters are presented in Table 1.

2.4. Optical Follow-up Observations

Since the Swift/BAT triggered GRB 240529A, a number of optical telescopes are follow-up to observe, such as the Gravitational-wave Optical Transient Observer (A. Kumar et al. 2024), SAO RAS 1 m telescope (A. S. Moskvitin et al. 2024), AZT-33IK telescope (N. Pankov et al. 2024), 1.3 m Devasthal Fast Optical Telescope (A. K. Ror et al. 2024), Skynet's 0.6 m RRRT telescope (D. Dutton et al. 2024), 50 cm-B, 50 cm-C, 100 cm-C telescopes (J. An et al. 2024). However, most optical telescope follow-up observations only present one more observed point or upper limits. So, we collect the observations of the *R* band, which is the most observed band from the GCN reports, and plot the optical light curve.

2.5. Redshift Measured of GRB 240529A

The spectroscopy of the afterglow of GRB 240529A is obtained by using OSIRIS at the 10.4 m GTC telescope in the Roque de los Muchachos Observatory, and the spectrum shows a bright continuum with many strong spectral features (A. de Ugarte Postigo et al. 2024). Based on the observed three absorption lines, they identified the redshift of GRB 240529A as $z = 2.695$, $z = 2.035$, and $z = 1.695$, respectively (A. de Ugarte Postigo et al. 2024).

By adopting the redshift of GRB 240529A as $z = 2.695$, $z = 2.035$, and $z = 1.695$, together with the fluence of three-episode emissions in the prompt emission and fitting results in X-ray afterglow emission, one can calculate the isotropic energy of three-episode emissions and two-plateau emissions (see Table 2),

$$E_{\gamma,\mathrm{iso,i}} = 4\pi D_L^2 f_i / (1+z), \quad (7)$$

where i = I, II, or III. We correct the isotropic energy of three-episode emissions to the beaming-correction values E_γ by

Table 2
Calculation Results of the Prompt and Afterglow Emissions of GRB 240529A

Redshift	I	II	III	First Plateau		Second Plateau	
	$E_{\gamma,\mathrm{iso,I}}$ (10^{52} erg)	$E_{\gamma,\mathrm{iso,II}}$ (10^{52} erg)	$E_{\gamma,\mathrm{iso,III}}$ (10^{52} erg)	$L_{\mathrm{b,iso,1}}$ (10^{48} erg s^{-1})	$E_{\mathrm{X,iso,1}}$ (10^{51} erg)	$L_{\mathrm{b,iso,2}}$ (10^{48} erg s^{-1})	$E_{\mathrm{X,iso,2}}$ (10^{51} erg)
$z = 2.695$	18.09 ± 1.53	3.18 ± 0.88	48.48 ± 0.73	48.79 ± 2.19	8.73 ± 0.40	1.08 ± 0.05	4.44 ± 0.23
$z = 2.035$	11.12 ± 0.94	1.96 ± 0.54	29.80 ± 0.05	29.99 ± 1.35	6.53 ± 0.30	0.67 ± 0.03	3.32 ± 0.17
$z = 1.695$	8.00 ± 0.68	1.41 ± 0.39	21.43 ± 0.32	21.56 ± 0.97	5.29 ± 0.24	0.48 ± 0.02	2.69 ± 0.14

considering a possible beaming-correction factor:

$$f_{\mathrm{b}} = 1 - \cos\theta_{\mathrm{j}} \simeq (1/2)\theta_{\mathrm{j}}^2, \tag{8}$$

where θ_{j} is the jet opening angle, and $E_{\gamma} = E_{\gamma,\mathrm{iso}} f_{\mathrm{b}}$.

The isotropic break luminosity at the break time of two-plateau emissions can be calculated by

$$L_{\mathrm{b,iso,j}} = 4\pi D_{\mathrm{L}}^2 F_{\mathrm{b,j}}/(1+z), \tag{9}$$

where $j = 1$ or 2 indicate the first and second plateau emission, respectively. Then, the isotropic energy of X-ray plateau emission, $E_{\mathrm{X,iso,j}}$, can be derived by employing the break time and break luminosity (H.-J. Lü & B. Zhang 2014),

$$E_{\mathrm{X,iso,j}} \simeq L_{\mathrm{b,iso,j}} \cdot \frac{t_{\mathrm{b,j}}}{(1+z)}. \tag{10}$$

One needs to note that the first-episode emission occurs before the BAT trigger time, about 407 s. So, the true break time of two-plateau emissions should be $t_{\mathrm{b,j}} + 407$ s. If this is the case, one can estimate the isotropic energy of two-plateau emissions, and the calculated results for different redshifts of GRB 240529A are also shown in Table 2.

3. Physical Interpretation

In this section, we invoke the supramassive magnetar as the central engine, phase transition from magnetar to strange star, and the cooling and spin-down of the strange star to interpret each observed segment of prompt emission and X-ray afterglow of GRB 240529A.

3.1. The First and Second Episode of Prompt Emission: Jet Radiation of Central Engine

The long-duration prompt gamma ray of GRB 240529A suggests that it is likely related to the deaths of massive stars. If this is the case, a hyperaccreting black hole, a rapidly spinning magnetar, or a strange star as the central engine may be formed (B. Zhang 2018). The central engine lasts long enough to allow the jet head to break out of the star, and a successful jet is produced. Based on the feature of X-ray afterglow discussed below, the supramassive magnetar with surface polar cap magnetic field B_{p} of about 10^{15} G and initial spin period P_0 of about 1 ms is a potential candidate as the central engine of GRB 240529A. The newborn millisecond magnetar will power the GRB jet by losing its huge total rotational energy E_{rot}.

Based on the method in B. Zhang & P. Mészáros (2001), the total rotational energy of the newborn millisecond magnetar can be expressed as:

$$E_{\mathrm{rot}} = \frac{1}{2} I \Omega_0^2 \approx 2 \times 10^{52}\ \mathrm{erg}\ M_{1.4} R_6^2 P_{0,-3}^{-2}, \tag{11}$$

where I is the moment of inertia; and Ω_0, $R = 10$ km and $M_{1.4} = M/1.4M_{\odot}$ are the initial angular frequency, radius and mass of the neutron star, respectively. There are three energy extraction mechanisms for a millisecond magnetar engine to power the GRB jet, such as rotation energy (S. L. Shapiro & S. A. Teukolsky 1983; B. Zhang & P. Mészáros 2001), magnetic bubble eruption due to differential rotation (W. Kluźniak & M. Ruderman 1998; M. A. Ruderman et al. 2000), and accretion of neutron stars (D. Zhang & Z. G. Dai 2008, 2009).

The isotropic energy $E_{\gamma,\mathrm{iso,I}}$ of the first episode of GRB 240529A prompt emission is about 2×10^{53} erg, 10^{53} erg, and 8×10^{52} erg at redshift $z = 2.695$, $z = 2.035$, and $z = 1.695$, respectively. Since the θ_{j} of GRB 240529A is unknown, we have to adopt a typical value of the beaming factor as $f_{\mathrm{b}} = 0.01$ to do the jet correction of $E_{\gamma,\mathrm{I}}$ (E.-W. Liang et al. 2008; J. L. Racusin et al. 2009; R. S. Nemmen et al. 2012; H.-J. Lü & B. Zhang 2014; H.-J. Lü et al. 2017). The values of $E_{\gamma,\mathrm{I}}$ for different redshifts $z = 2.695$, 2.035, and 1.695 can be estimated as 2×10^{51} erg, 10^{51} erg, and 8×10^{50} erg, respectively. On the one hand, the total energy budget of the newborn magnetar can be satisfied with the observed energy released in the first episode of prompt gamma-ray emission. On the other hand, together with considering the feature of two X-ray plateau emissions discussed below, it suggests that the first episode of prompt emission is possibly produced by the supramassive magnetar central engine from the death of a massive star.

The intensity of the second-episode emission is 5 times less than that of the first-episode emission, and this feature is not surprising in the prompt emission of GRBs (T. M. Koshut et al. 1995; D. Lazzati 2005; M. G. Bernardini et al. 2013; Y.-D. Hu et al. 2014; L. Lan et al. 2018). L. Lan et al. (2018) showed that there are not any significant differences in the spectral and temporal properties of these two subburst emissions and suggested that these two subburst emissions likely share the same physical origin. On the other hand, the X-ray flares have been discovered in a good fraction of GRBs afterglow (D. N. Burrows et al. 2005; G. Chincarini et al. 2007; R. Margutti et al. 2010). Temporal and spectral analyses of X-ray flares reveal many properties analogous to prompt emission and suggest that X-ray flares are directly powered by the GRB central engine, similar to prompt emission. They are the extension and delay of prompt emission, and are possible from the later reactivity of the central engine (D. N. Burrows et al. 2005; Y. Z. Fan & D. M. Wei 2005; B. Zhang et al. 2006).

If the second-episode emission of GRB 240529A is indeed from the later central engine reactivity. Generally speaking, in order to produce a second "burst" as is observed in GRB 240529A, the central engine must restart about one-fifth

of the energy by comparing the first burst. Several models are proposed to interpret such subburst in the prompt emission of GRBs, such as fragmentation in the massive star envelope (A. King et al. 2005), fragmentation in the accretion disk (R. Perna et al. 2006), the magnetic barrier around the accretor (D. Proga & B. Zhang 2006), fallback accretion of a newborn millisecond magnetar (A. L. Piro & C. D. Ott 2011; B. P. Gompertz et al. 2014; S. L. Gibson et al. 2017, 2018; L. Lan et al. 2020; W.-Y. Yu et al. 2024).

However, those models also predict that the X-ray flares should be produced at a late time, but we do not observe any flares in the X-ray afterglow. Two ways may be used to solve the above inconsistency: one is that it indeed produces the X-ray flares sometimes before the magnetar transforms into a strange star, but XRT does not start to observe; The other one is that the produced X-ray flares are too weak to be detected by XRT. In any case, the later central engine reactivity model is not contradictory to the observations of the second episode for GRB 240529A.

3.2. The Third Episode of Prompt Emission: Phase Transition from Magnetar to Strange Star

Theoretically, the strange star has an extremely high density, and a three-flavor (*uds*) quark–gluon plasma is more stable than baryons and a two-flavor (*ud*) QGP. An entire neutron star may be converted to a star made of strange quark matter. The release of a substantial amount of energy during NS → SS phase transition to power the GRB prompt emission has been extensively researched as a potential energy source of GRBs (K. S. Cheng & Z. G. Dai 1996; Z. G. Dai & T. Lu 1998b; R. Ouyed & F. Sannino 2002).

Therefore, in this section, we propose that the third-episode emission of GRB 240529A prompt emission is powered by the phase transition from a neutron star to a strange star. The possible physical process can be described as follows:

(a) The neutron star formed by the gravitational collapse of a massive star results in an increasing density of its center via accretion. Once the central density reaches the critical value for the quark deconfinement phase transition, a seed of SQM will be generated within the core. This process takes about a few milliseconds.

(b) Then, due to the production and diffusion of these seeds of SQM, a neutron star transforms into a strange star after tens of seconds. The surface layer of the newborn SS is very hot, with a temperature $\sim 10^{11}$ K.

(c) The baryonic material can be ablated again from the newborn SS surface as long as the surface is not completely filled with strange quark matter (A. Drago & G. Pagliara 2016). In this way, a new gamma-ray emission can be produced by the strange star.

Here, we assume that the generated strange star has a mass of $M_{\rm SS} = 2.5\,M_{\odot}$ (about 5×10^{33} g), and it includes the total baryon number $n \sim 2.5 \times 10^{57}$. If each nucleon can release 50 MeV heat energy during the phase transition, the expected energy can be estimated as

$$E_{\rm conv} \sim 50 \times 2.5 \times 10^{57}\,{\rm MeV} = 2 \times 10^{53}\,{\rm erg}. \quad (12)$$

On the other hand, by considering the different equation of state of NS and SS, I. Bombaci et al. (2000) provided that the energy released during the phase transition range of $(1–4) \times 10^{53}$ erg.

Observationally, the calculated isotropic energy of the third-episode emission of prompt gamma-ray $E_{\gamma,{\rm iso,III}}$, are about 5×10^{53} erg, 3×10^{53} erg, and 2×10^{53} erg at redshift $z = 2.695$, $z = 2.035$, and $z = 1.695$, respectively. By considering the beaming-correction factor $f_{\rm b} = 0.01$, one can obtain the beaming-corrected energy $E_{\gamma,{\rm III}}$ of this episode, which is in the range of $(2–5) \times 10^{51}$ erg. It is consistent with that of energy predicted during phase transition for energy conversion efficiency $\epsilon = 0.01$. It means that the phase transition at least from the side of energy released could reasonably explain the third-episode emission of GRB 240529A prompt emission. If this is the case, a supramassive strange star as the central engine of GRB 240529A may survive to drive third-episode gamma-ray emission.

3.3. The First Plateau Emission of X-Ray Afterglow: Cooling of Strange Star

Initially, a newborn strange star may be in the liquid phase due to its high temperature. The liquid strange star will transition into a solid state when the temperature is decreased due to the energy released by cooling (R. X. Xu 2003; R. Xu & E. Liang 2009). The latent heat released energy during the cooling is proposed to explain the observed X-ray plateau followed by a rapid decay phase in GRBs (or internal plateau), and this latent heat released is injected into the GRB afterglow through a mechanism, which is similar to a Poynting flux-dominated outflow (S. Dai et al. 2011; S.-J. Hou et al. 2018).

Based on the solid SS model proposed by X. Y. Lai & R. X. Xu (2009), one can calculate the released energy (E) by each baryon during the transition from liquid to solid of the strange star. By fixing the depth of the potential $U_0 = 100$ MeV, and the ratio between melting heat and the potential $f_{\rm mp} \approx 0.01–0.1$ (S. Dai et al. 2011), it can be written as

$$E \sim f_{\rm mp}\,U_0 \approx (1 - 10)\,{\rm MeV}. \quad (13)$$

For $M_{\rm SS} = 2.5\,M_{\odot}$ with $n \sim 2.5 \times 10^{57}$ of the strange star, the total released energy during cooling can be estimated as

$$E_{\rm cooling} = nE \approx (0.4–4) \times 10^{52}\,{\rm erg}. \quad (14)$$

By considering the energy conversion efficiency $\xi = 0.2$ from cooling energy to X-ray emission, the radiation energy in X-ray emission should be in the range of $(0.8–8) \times 10^{51}$ erg. Moreover, the observed isotropic energy of the first plateau emission $E_{\rm X,iso,1}$ of X-ray afterglow for GRB 240529A is distributed within the range of $(5–9) \times 10^{51}$ erg at three different redshifts ($z = 2.695$, 2.035, and 1.695). It is found that the cooling energy released is consistent with the observed X-ray emission of GRB 240529A.

On the other hand, the radiation timescale for the strange star can be estimated as follows by assuming blackbody radiation:

$$t = \frac{E_{\rm cooling}}{L_{\rm rad}} = \frac{E_{\rm cooling}}{\sigma T^4 4\pi R^2}, \quad (15)$$

where σ and T are the Stefan–Boltzman constant and temperature of the blackbody, respectively. R is the radius of the newborn SS. More significantly, when the strange star is cooling from liquid to solid phase, the radiation luminosity $L_{\rm rad}$ is almost constant because the temperature is not changed. So it would appear a plateau emission in the light curve of X-ray afterglow. At the end of the cooling, the energy injection will

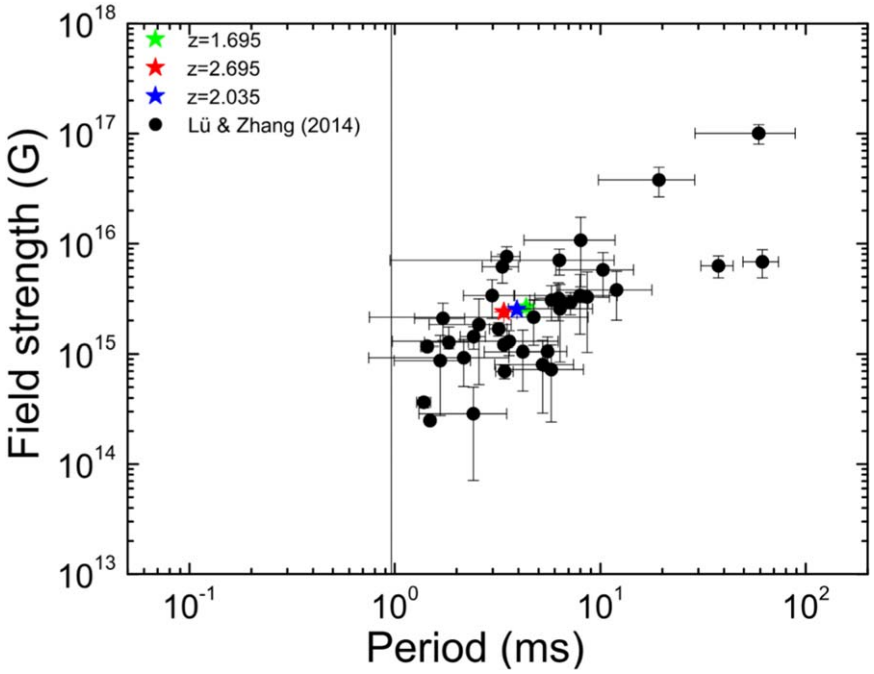

Figure 3. Inferred strange star parameters of GRB 240529A, initial spin period P_0 vs. surface polar cap magnetic field strength B_p derived for different redshifts. The candidates for the magnetar central engine are taken from H.-J. Lü & B. Zhang (2014). The vertical solid line is the breakup spin period for a neutron star (J. M. Lattimer & M. Prakash 2004).

be abruptly cut off because the solid SS with low heat capacity is cooling very fast. By adopting the duration of plateau timescale $t = t_{b,1} \sim 661$ s and conversion efficiency $\xi = 0.2$, one can estimate the temperature $kT \sim 2$ MeV, 1.85 MeV, and 1.7 MeV at different redshift $z = 2.695$, 2.035, and 1.695, respectively. It is natural to explain the presence of a plateau with a rapid decay (first plateau) phase in the X-ray light curve.

3.4. The Second Plateau Emission of X-Ray Afterglow: Magnetic Dipole Radiation of Strange Star Spin-down

After the strange star cooling, the newborn strange star has cooled to a solid crystal. We consider that the properties of the solid SS are similar to that of the magnetar. The strange star with rapid spinning as the GRB central engine can also lose its rotational energy mainly via two mechanisms, i.e., electromagnetic (EM) dipole and gravitational-wave (GW) radiations (B. Zhang & P. Mészáros 2001; Y.-Z. Fan et al. 2013; P. D. Lasky & K. Glampedakis 2016). For EM dominated, the temporal evolution of the EM luminosity $L_{\rm EM}$ can be formulated as (P. D. Lasky & K. Glampedakis 2016; H.-J. Lü et al. 2018)

$$L_{\rm EM} = L_0(1 + t/\tau_{\rm EM})^{-2}. \quad (16)$$

For GW dominated, the temporal evolution of the GW luminosity $L_{\rm GW}$ can be expressed as

$$L_{\rm GW} = L_0(1 + t/\tau_{\rm GW})^{-1}. \quad (17)$$

Here, L_0 is the characteristic spin-down luminosity. $\tau_{\rm EM}$ and $\tau_{\rm GW}$ are characteristic spin-down timescales for the case of EM dominated and GW dominated, respectively.

We note that the decay index of the second plateau emission is about $L \propto t^{-2}$ based on the fitting in Section 2.3, and it is consistent with the case of energy loss dominated by EM dipole radiation. The $\tau_{\rm EM}$ and L_0 can be expressed as

$$\tau_{\rm EM} = 2.05 \times 10^3\, I_{45} B_{p,15}^{-2} P_{0,-3}^{2} R_6^{-6}\ {\rm s}, \quad (18)$$

$$L_0 = 1.0 \times 10^{49}\, B_{p,15}^{2} P_{0,-3}^{-4} R_6^{6}\ {\rm erg\ s^{-1}}. \quad (19)$$

For EM dominated, we adopt $L_{\rm EM} \approx L_0$, and the isotropic break luminosity $L_{\rm b,iso,2}$ of the second plateau emission is about 1.08×10^{48} erg, 0.67×10^{48} erg, and 0.48×10^{48} erg at redshift $z = 2.695$, 2.035, and 1.695, respectively. Here, after the jet correction of break luminosity $L_{\rm b,2}$ can be expressed as $L_{\rm b,2} = L_{\rm b,iso,2} f_{\rm b}$. By considering the energy conversion efficiency ($\eta = 0.01$) from strange star spin-down to the X-ray emission, the break luminosity of the second plateau emission can be written as $L_{\rm b,2} = \eta L_0$. Based on Equations (18) and (19), by adopting the characteristic spin-down timescale $\tau_{\rm EM} \sim t_{\rm b,2}/(1+z)$ and conversion efficiency $\eta = 0.01$, together with the observed second plateau luminosity of X-ray afterglow, one can constrain the characteristic parameters of the strange star. In order to compare the difference between the strange star as the central engine of GRB 240529A and other candidates of magnetar central engine of LGRBs from H.-J. Lü & B. Zhang (2014), we similarly adopt the jet opening angle to be 5°, and then do the jet correction of the derived B_p and P_0 for GRB 240529A. One has $B_p = (2.40 \pm 0.14) \times 10^{15}$ G and $P_0 = 3.40 \pm 0.09$ ms at redshift $z = 2.695$, $B_p = (2.52 \pm 0.14) \times 10^{15}$ G and $P_0 = 3.93 \pm 0.10$ ms at redshift $z = 2.035$, and $B_p = (2.64 \pm 0.15) \times 10^{15}$ G and $P_0 = 4.36 \pm 0.11$ ms at redshift $z = 1.695$. Figure 3 shows the distribution of $B_{\rm p}$ and P_0 of GRB 240529A with different redshifts and compares it with other candidates of magnetar central engine of LGRBs from H.-J. Lü & B. Zhang (2014). We find that the derived $B_{\rm p}$ and P_0 fall into the reasonable range at different redshifts and mix with those of the other

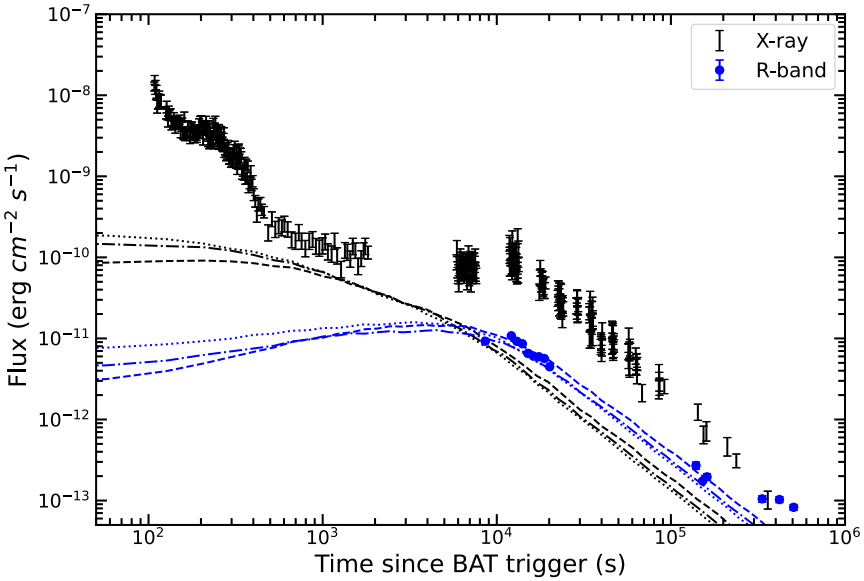

Figure 4. The fitting results with external shock model in X-ray and optical bands of GRB 240529A. The standard afterglow model parameters show as: $\Gamma = 71$, $n = 10$, $\epsilon_e = \epsilon_B = 0.08$ and $p = 2.8$. Here, the initial total kinetic energy $E_{K,iso}$ is about 5×10^{52} erg, 2.5×10^{52} erg, and 2.0×10^{52} erg at redshift $z = 2.695$ (dashed line), 2.035 (dashed–dotted line), and 1.695 (dotted line), respectively.

LGRB candidates with magnetar central engine from H.-J. Lü & B. Zhang (2014).

4. Conclusion and Discussion

GRB 240529A is a long-duration GRB that was detected by Swift, Insight-HXMT, as well as the Konus-Wind (R. A. J. Eyles-Ferris et al. 2024; D. Svinkin et al. 2024; W. Tan et al. 2024). The possible redshift of GRB 240529A is identified as $z = 2.695$, 2.035, and 1.695, based on three absorption lines in the spectrum (A. de Ugarte Postigo et al. 2024). Insight-HXMT/HE detected GRB 240529A in a routine data search; it was earlier than the triggered time of Swift/BAT, about 407 s (W. Tan et al. 2024). The prompt emission of GRB 240529A detected by Insight-HXMT is composed of a triple-episode structure, separated by quiescent gaps of tens to hundreds of seconds. Only the third-episode emission is simultaneously observed by both Swift/BAT and Insight-HXMT. By extracting the time-averaged spectrum of each episode of the prompt emission of GRB 240529A, we find that a simple power-law model can best fit the first two episodes, while the third episode can be adequately fitted by a cutoff power-law model with $E_p = 584^{+102}_{-74}$ keV.

More interestingly, the X-ray afterglow light curve of GRB 240529A exhibits the behavior of a steep decay phase and two plateau phases. We adopt an MCMC method to fit the light curve by invoking one power-law + two smooth broken power-law models. The first segment is a power-law decay with the temporal index $\alpha_1 = 9.09 \pm 1.45$ that is consistent with the tail emission of the prompt gamma ray due to the curvature effect (P. Kumar & A. Panaitescu 2000; B.-B. Zhang et al. 2007; Z. L. Uhm & B. Zhang 2015). The first plateau emission with the temporal decay index and the break time are $\alpha_2 = 0.25 \pm 0.18$, $\alpha_3 = 3.89 \pm 0.15$, and $t_{b,2} = 254 \pm 5$ s, which is consistent with the internal plateau. The temporal decay indices of the second plateau before and after the break time $t_{b,3} = 14703 \pm 401$ s are $\alpha_4 = 0.09 \pm 0.04$ and $\alpha_5 = 1.95 \pm 0.03$, respectively.

Such a feature of three episodes in the prompt emission of GRB 240529A, together with two plateau emissions in the X-ray afterglow, suggests that the standard internal/external shock model of a black hole central engine is very difficult to explain both the prompt emission and X-ray afterglow of GRB 240529A. However, it could be more consistent with the prediction of a supermassive magnetar as a central engine, the physical process of magnetar collapse into a strange star, and the cooling and spin-down of a strange star.

In this paper, we propose the above physical picture to interpret each observed segment in both the prompt emission and X-ray afterglow of GRB 240529A and it is summarized as follows:

(1) A supramassive magnetar as the central engine may be formed after the death of a massive star. The central engine lasts long enough to allow the jet head to break out of the star, and a successful jet is produced by losing its huge total rotational energy E_{rot}. This is naturally to explain the first episode of prompt emission. Then, the central engine is reactivity to power a weak subburst via fragmentation in the accretion disk (R. Perna et al. 2006), magnetic barrier around the accretor (D. Proga & B. Zhang 2006), or fallback of magnetar (A. L. Piro & C. D. Ott 2011; B. P. Gompertz et al. 2014; S. L. Gibson et al. 2017, 2018; L. Lan et al. 2020; W.-Y. Yu et al. 2024). It can be used to explain the second-episode emission of prompt emission of GRB 240529A.

(2) Theoretically, the strange star is more stable than the neutron star, and a substantial amount of energy may be released when a magnetar transitions into a strange star via quark deconfinement phase transition. The third-episode emission of a prompt gamma ray can be powered by the phase transition from a neutron star to a strange star.

(3) Initially, a newborn strange star may be in the liquid phase due to its high temperature. The energy lost via some cooling mechanisms can result in the newborn strange star transforming from liquid to solid state. It predicts a plateau emission followed by an extremely sharp decay, which is

consistent with the observations of the first plateau emission of X-ray afterglow.

(4) After the strange star cooling, the newborn strange star has cooled to a solid crystal. The properties of the solid strange star are similar to those of the magnetar. The strange star with rapid spinning as the GRB central engine can also lose its rotational energy mainly via magnetic dipole radiation. The model predicts that the temporal evolution of the EM luminosity is $L_{\rm EM} = L_0(1 + t/\tau_{\rm EM})^{-2}$, which is consistent with the observed second plateau emission of X-ray afterglow.

If this is the case, we also infer the magnetic field strength $B_{\rm p}$ and initial spin period P_0 of the strange star of GRB 240529A, and compare these values with other candidates of magnetar central engine for LGRBs from H.-J. Lü & B. Zhang (2014). We find that the derived $B_{\rm p}$ and P_0 fall into the reasonable range at different redshifts and mix with those of other LGRB candidates with a magnetar central engine.

If the observed prompt emission and X-ray afterglow are all attributed to internal dissipation, one question is, where is the external component when the ejecta interact with the interstellar medium? In order to answer this question, we collect the observed optical data in the R band, which are the most data points released from the GCN report (J. An et al. 2024; D. Dutton et al. 2024; A. Kumar et al. 2024; A. S. Moskvitin et al. 2024; N. Pankov et al. 2024; A. K. Ror et al. 2024). The optical light curve shows an initial bump connected to a normal decay, and it seems to be contributed from the external shock model. Therefore, we adopt the standard afterglow model to fit the optical light curves for three different redshifts (R. Sari et al. 1998; Y. F. Huang et al. 1999), and the fitting results are shown in Figure 4. One can obtain the parameters of the external shock model as the initial Lorentz factor $\Gamma = 71$, the circumburst medium density $n = 10$, the equipartition parameters $\epsilon_{\rm e} = \epsilon_{\rm B} = 0.08$, and the electron injection spectral index $p = 2.8$. The initial total kinetic energy $E_{\rm K,iso}$ is about 5×10^{52} erg, 2.5×10^{52} erg, 2.0×10^{52} erg at redshift $z = 2.695$, 2.035, and 1.695, respectively. We find that the external component in X-ray afterglow still exists, but it is too faint to be detected by comparing it with internal dissipation.

Moreover, the physical explanation of GRB 240529A that we adopted may not be the only one to the observations, but it should be the most self-consistent explanation with the observations. For example, T.-R. Sun et al. (2024) invoked two shocks launched from the central engine separately to explain the multiwavelength emissions of GRB 240529A, but did not explain the first X-ray plateau emission. Also, Y. Aimuratov et al. (2023) recently proposed to adopt a binary-driven hypernova model to explain GRB 171205A, whose X-ray light curve (e.g., a two-plateau emission with sparse data) is quite similar to that of GRB 240529A, but is not related to the three-episode emission in prompt emission (R. Ruffini et al. 2014). X.-Y. Wang & P. Mészáros (2007) proposed the jet bow shock and relativistic jet itself to explain two-episode emission, but it is not related to two-plateau X-ray emissions. V. M. Lipunov & E. S. Gorbovskoy (2008) proposed a simple nonstationary three-parameter collapse model to explain both precursors and X-ray plateau emission or continues to eject relativistic material from the central engine (F. Nappo et al. 2014).

On the other hand, two interesting questions naturally arise. One is why it occurs in GRB 240529A and not in every GRB. For this question, there are two possible ways to interpret it, such as the probability of a massive star collapsing into a black hole and then producing GRBs is slightly higher than that of collapsing into a magnetar to produce GRBs (H.-J. Pankov et al. 2022), or the strict requirements for the initial mass of a massive star and the equation of state of a neutron star. Another one is how identifying the central engine (e.g., neutron star or black hole) of GRBs through electromagnetic observations is an extremely challenging task. Recently, C. Fransson et al. (2024) confirmed that the central engine of SN 1987A is a neutron star with the observed narrow infrared emission lines of argon and sulfur from the James Webb Space Telescope (JWST). Moreover, the GRB 170817A/GW170817 event from the merger of neutron stars is currently the only example of joint electromagnetic and gravitational-wave observations to confirm a Kerr black hole as the central engine (M. H. P. M. van Putten & M. Della Valle 2023). For the long-duration GRBs, we expect to detect both electromagnetic and gravitational waves for the same burst event in the future, and it will provide decisive evidence to answer this question.

Acknowledgments

We acknowledge the use of the public data from the Swift Science Data Center. This work is supported by the Guangxi Science Foundation (grant No. 2023GXNSFDA026007), the Natural Science Foundation of China (grant Nos. 12494574, 11922301, and 12133003), the Program of Bagui Scholars Program (LHJ), and the Guangxi Talent Program ("Highland of Innovation Talents"). S.Q.Z is supported by the starting Foundation of Guangxi University of Science and Technology (grant No. 24Z17).

ORCID iDs

HouJun Lü https://orcid.org/0000-0001-6396-9386
ShaoLin Xiong https://orcid.org/0000-0002-4771-7653
ShuQing Zhong https://orcid.org/0000-0002-1766-6947
EnWei Liang https://orcid.org/0000-0002-7044-733X

References

Abbott, B. P., Abbott, R., Abbott, T. D., et al. 2017, PhRvL, 119, 161101
Aimuratov, Y., Becerra, L. M., Bianco, C. L., et al. 2023, ApJ, 955, 93
Alcock, C., Farhi, E., & Olinto, A. 1986, ApJ, 310, 261
An, J., Liu, X., Zhu, Z. P., et al. 2024, GCN, 36734, 1
Berezhiani, Z., Bombaci, I., Drago, A., et al. 2003, ApJ, 586, 1250
Berger, E., Fong, W., & Chornock, R. 2013, ApJL, 774, L23
Bernardini, M. G., Campana, S., Ghisellini, G., et al. 2013, ApJ, 775, 67
Bombaci, I., Parenti, I., & Vidaña, I. 2004, ApJ, 614, 314
Bombaci, I., Thampan, A. V., & Datta, B. 2000, ApJL, 541, L71
Bromberg, O., Nakar, E., Piran, T., et al. 2013, ApJ, 764, 179
Bucciantini, N., Metzger, B. D., Thompson, T. A., et al. 2012, MNRAS, 419, 1537
Burrows, D. N., Romano, P., Falcone, A., et al. 2005, Sci, 309, 1833
Cenko, S. B., Frail, D. A., Harrison, F. A., et al. 2011, ApJ, 732, 29
Cheng, K. S., & Dai, Z. G. 1996, PhRvL, 77, 1210
Chincarini, G., Moretti, A., Romano, P., et al. 2007, ApJ, 671, 1903
Coppin, P., de Vries, K. D., & van Eijndhoven, N. 2020, PhRvD, 102, 103014
Dai, S., Li, L., & Xu, R. 2011, SCPMA, 54, 1541
Dai, Z. G., & Lu, T. 1998a, A&A, 333, L87
Dai, Z. G., & Lu, T. 1998b, PhRvL, 81, 4301
de Ugarte Postigo, A., Thoene, C. C., Agui Fernandez, J. F., et al. 2024, GCN, 36574, 1
Dichiara, S., Kennea, J. A., Page, K. L., et al. 2024, GCN, 36564, 1
Drago, A., & Pagliara, G. 2016, EPJA, 52, 41
Dutton, D., Reichart, D., Haislip, J., et al. 2024, GCN, 36568, 1
Eyles-Ferris, R. A. J., Gupta, R., Lien, A. Y., et al. 2024, GCN, 36556, 1
Farhi, E., & Jaffe, R. L. 1984, PhRvD, 30, 2379
Fan, Y. Z., & Wei, D. M. 2005, MNRAS, 364, L42

Fan, Y.-Z., Wu, X.-F., & Wei, D.-M. 2013, PhRvD, 88, 067304
Fransson, C., Barlow, M. J., Kavanagh, P. J., et al. 2024, Sci, 383, 898
Galama, T. J., Vreeswijk, P. M., van Paradijs, J., et al. 1998, Natur, 395, 670
Gibson, S. L., Wynn, G. A., Gompertz, B. P., et al. 2017, MNRAS, 470, 4925
Gibson, S. L., Wynn, G. A., Gompertz, B. P., et al. 2018, MNRAS, 478, 4323
Gompertz, B. P., O'Brien, P. T., & Wynn, G. A. 2014, MNRAS, 438, 240
Haensel, P., & Zdunik, J. L. 2006, NCimB, 121, 1349
Herzog, M., & Röpke, F. K. 2011, PhRvD, 84, 083002
Hou, S.-J., Liu, T., Xu, R.-X., et al. 2018, ApJ, 854, 104
Hu, Y.-D., Liang, E.-W., Xi, S.-Q., et al. 2014, ApJ, 789, 145
Huang, Y. F., Dai, Z. G., & Lu, T. 1999, MNRAS, 309, 513
Jin, Z.-P., Hotokezaka, K., Li, X., et al. 2016, NatCo, 7, 12898
Kelly, P. L., & Kirshner, R. P. 2012, ApJ, 759, 107
Kelly, P. L., Kirshner, R. P., & Pahre, M. 2008, ApJ, 687, 1201
King, A., O'Brien, P. T., Goad, M. R., et al. 2005, ApJL, 630, L113
Kluźniak, W., & Ruderman, M. 1998, ApJL, 505, L113
Kouveliotou, C., Meegan, C. A., Fishman, G. J., et al. 1993, ApJL, 413, L101
Koshut, T. M., Kouveliotou, C., Paciesas, W. S., et al. 1995, ApJ, 452, 145
Kumar, A., Gompertz, B. P., Belkin, S., et al. 2024, GCN, 36559, 1
Kumar, P., & Panaitescu, A. 2000, ApJL, 541, L51
Kumar, P., & Zhang, B. 2015, PhR, 561, 1
Lai, X. Y., & Xu, R. X. 2009, MNRAS, 398, L31
Lamb, G. P., Lyman, J. D., Levan, A. J., et al. 2019, ApJL, 870, L15
Lan, L., Lu, R.-J., Lü, H.-J., et al. 2020, MNRAS, 492, 3622
Lan, L., Lü, H.-J., Zhong, S.-Q., et al. 2018, ApJ, 862, 155
Lasky, P. D., & Glampedakis, K. 2016, MNRAS, 458, 1660
Lattimer, J. M., & Prakash, M. 2004, Sci, 304, 536
Lazzati, D. 2005, MNRAS, 357, 722
Lei, W.-H., Zhang, B., & Liang, E.-W. 2013, ApJ, 765, 125
Li, A., Zhang, B., Zhang, N.-B., et al. 2016, PhRvD, 94, 083010
Liang, E.-W., Racusin, J. L., Zhang, B., et al. 2008, ApJ, 675, 528
Liang, E.-W., Zhang, B.-B., & Zhang, B. 2007, ApJ, 670, 565
Lipunov, V. M., & Gorbovskoy, E. S. 2008, MNRAS, 383, 1397
Liu, T., Gu, W.-M., & Zhang, B. 2017, NewAR, 79, 1
Lü, H.-J., Liang, E.-W., Zhang, B.-B., et al. 2010, ApJ, 725, 1965
Lü, H.-J., & Zhang, B. 2014, ApJ, 785, 74
Lü, H.-J., Zhang, B., Lei, W.-H., et al. 2015, ApJ, 805, 89
Lü, H.-J., Zhang, H.-M., Zhong, S.-Q., et al. 2017, ApJ, 835, 181
Lü, H.-J., Zou, L., Lan, L., et al. 2018, MNRAS, 480, 4402
Luo, Q., Liao, J.-Y., Li, X.-F., et al. 2020, JHEAp, 27, 1
Lyons, N., O'Brien, P. T., Zhang, B., et al. 2010, MNRAS, 402, 705
Malesani, D., Tagliaferri, G., Chincarini, G., et al. 2004, ApJL, 609, L5
Margutti, R., Guidorzi, C., Chincarini, G., et al. 2010, MNRAS, 406, 2149
Markwardt, C. B., Barthelmy, S. D., Gupta, R., et al. 2024, GCN, 36566, 1
Metzger, B. D. 2019, LRR, 23, 1
Metzger, B. D., Giannios, D., Thompson, T. A., et al. 2011, MNRAS, 413, 2031
Mintz, B. W., Fraga, E. S., Pagliara, G., et al. 2010, PhRvD, 81, 123012
Modjaz, M., Stanek, K. Z., Garnavich, P. M., et al. 2006, ApJL, 645, L21
Moskvitin, A. S., Maslennikova, O. A., Spiridonova, O. I., et al. 2024, GCN, 36601, 1
Nappo, F., Ghisellini, G., Ghirlanda, G., et al. 2014, MNRAS, 445, 1625
Nemmen, R. S., Georganopoulos, M., Guiriec, S., et al. 2012, Sci, 338, 1445
Nousek, J. A., Kouveliotou, C., Grupe, D., et al. 2006, ApJ, 642, 389
Olinto, A. V. 1987, PhLB, 192, 71
Ouyed, R., Leahy, D., & Koning, N. 2020, RAA, 20, 027
Ouyed, R., Rapp, R., & Vogt, C. 2005, ApJ, 632, 1001
Ouyed, R., & Sannino, F. 2002, A&A, 387, 725
Pankov, H.-J., Kim, S.-J., Kim, S., et al. 2022, ApJ, 938, 69
Pankov, N., Pozanenko, A., Klunko, E., et al. 2024, GCN, 36585, 1
Perna, R., Armitage, P. J., & Zhang, B. 2006, ApJL, 636, L29
Pian, E., Mazzali, P. A., Masetti, N., et al. 2006, Natur, 442, 1011
Pili, A. G., Bucciantini, N., Drago, A., et al. 2016, MNRAS, 462, L26
Piro, A. L., & Ott, C. D. 2011, ApJ, 736, 108
Popham, R., Woosley, S. E., & Fryer, C. 1999, ApJ, 518, 356
Proga, D., & Zhang, B. 2006, MNRAS, 370, L61
Racusin, J. L., Liang, E. W., Burrows, D. N., et al. 2009, ApJ, 698, 43
Raskin, C., Scannapieco, E., Rhoads, J., et al. 2008, ApJ, 689, 358
Ror, A. K., Gupta, A., Rishi, C., et al. 2024, GCN, 36589, 1
Rowlinson, A., O'Brien, P. T., Metzger, B. D., et al. 2013, MNRAS, 430, 1061
Ruderman, M. A., Tao, L., & Kluźniak, W. 2000, ApJ, 542, 243
Ruffini, R., Muccino, M., Bianco, C. L., et al. 2014, A&A, 565, L10
Sakamoto, T., Barthelmy, S. D., Barbier, L., et al. 2008, ApJS, 175, 179
Sari, R., Piran, T., & Narayan, R. 1998, ApJL, 497, L17
Shapiro, S. L., & Teukolsky, S. A. 1983, JBAA, 93, 276
Stanek, K. Z., Matheson, T., Garnavich, P. M., et al. 2003, ApJL, 591, L17
Sun, T.-R., Geng, J.-J., Yan, J.-Z., et al. 2024, ApJL, 976, L20
Svinkin, D., Frederiks, D., Ulanov, M., et al. 2024, GCN, 36584, 1
Tan, W., Xiong, S., Li, X., et al. 2024, GCN, 36578, 1
Thompson, C. 1994, MNRAS, 270, 480
Troja, E., Cusumano, G., O'Brien, P. T., et al. 2007, ApJ, 665, 599
Uhm, Z. L., & Zhang, B. 2015, ApJ, 808, 33
Usov, V. V. 1992, Natur, 357, 472
van Putten, M. H. P. M., & Della Valle, M. 2023, A&A, 669, A36
Wang, X.-Y., & Mészáros, P. 2007, ApJ, 670, 1247
Weber, F. 2005, PrPNP, 54, 193
Witten, E. 1984, PhRvD, 30, 272
Xu, R., & Liang, E. 2009, ScChG, 52, 315
Xu, R. X. 2003, ApJL, 596, L59
Yu, W.-Y., Lü, H.-J., Yang, X., et al. 2024, ApJ, 962, 6
Zhang, B. 2006, Natur, 444, 1010
Zhang, B. 2011, CRPhy, 12, 206
Zhang, B. 2018, The Physics of Gamma-Ray Bursts by Bing Zhang, Vol. 2018 (Cambridge: Cambridge Univ. Press)
Zhang, B., Fan, Y. Z., Dyks, J., et al. 2006, ApJ, 642, 354
Zhang, B., & Mészáros, P. 2001, ApJL, 552, L35
Zhang, B.-B., Liang, E.-W., & Zhang, B. 2007, ApJ, 666, 1002
Zhang, D., & Dai, Z. G. 2009, ApJ, 703, 461
Zhang, D., & Dai, Z. G. 2008, ApJ, 683, 329
Zhang, S.-N., Li, T., Lu, F., et al. 2020, SCPMA, 63, 249502